Applied Physics Express 12, 056001 (2019)
https://doi.org/10.7567/1882-0786/ab18b5

LETTER

Fast-neutron irradiation effects on monolayer MoS_2

Ge Tang[1,2], Mei Er Pam[3,4], Hui Zhang[2], Zhiwen Shu[5], Peng Feng[1,6], Biao Wei[1*], LayKee Ang[3,4], Hui Ying Yang[3], and Mo Li[2*]

[1]Key Laboratory of Optoelectronic Technology and Systems, Ministry of Education, Chongqing University, Chongqing 400044, People's Republic of China
[2]Microsystems and Terahertz Research Center, China Academy of Engineering Physics, Chengdu 610200, People's Republic of China
[3]Pillar of Engineering Product Development, Singapore University of Technology and Design, Singapore 487372, Singapore
[4]Science and Math Cluster, Singapore University of Technology and Design, 8 Somapah Road, Singapore 487372, Singapore
[5]College of Mechanical and Vehicle Engineering, Hunan University, Changsha 410082, People's Republic of China
[6]Collaborative Innovation Center for Brain Science, Chongqing University, Chongqing, 400044, People's Republic of China

*E-mail: limo@mtrc.ac.cn; weibiao@cqu.edu.cn

Received February 24, 2019; revised April 8, 2019; accepted April 12, 2019; published online May 1, 2019

We investigated neutron irradiation effects on monolayer MoS_2 by photoluminescence (PL), Raman and X-ray photoelectron spectroscopy. Results revealed that Mo and S defects and oxidation replacements of S vacancies were generated by neutron irradiation, leading to the red-shifts and broadenings of the E^1_{2g} and A_{1g} Raman modes, as well as the red-shift of the A-exciton peak and quenching in the PL spectra. The relative atomic content ratio of S to Mo decreased with the increase of neutron flux, indicating that the neutron irradiation assisted in the release of S atoms.

Supplementary material for this article is available online

As the most common transition metal dichalcogenide, MoS_2 has attracted extensive attention due to its distinctive band structure,[1)] semiconducting[2)] or superconducting[3)] properties, and outstanding mechanical capabilities.[4)] It is well known that radiation can change the electronic structures or create defects in two-dimensional materials (2DMs) and further affect their electronic and optical performance.[5)] Tolerance to radiation and accompanying defect engineering are important considerations for the application of MoS_2 devices (e.g., as ultrathin transistors[6)] and chemical sensors[7)]) in nuclear and space environments. Recently, the effects of ion irradiation,[8,9)] laser irradiation,[10–12)] and gamma-ray irradiation[13)] on MoS_2 have been discussed. However, studies on neutron irradiation,[14–16)] one of the most common types of irradiation, and the damage it causes to MoS_2 are still lacking.[5)] Investigation of neutron effects can help in understanding the behaviors of MoS_2 devices used in nuclear and space environments and promote other fundamental researches such as those on neutron scattering.[17)]

A neutron is an uncharged elemental particle; it is not affected by the electric field around the nucleus. Neutrons with energies from 0.1 to 200 MeV are the most common radiation in space environments. The neutron source we use has an average energy of 1.2 MeV which is approximate to the space neutron energy spectrum. These fast neutrons do not directly cause the ionization and excitation of atoms as charged particles do, but create defects in materials by primary collision[5,18)] and cascading scattering events.[19)] Because 2DMs are of monolayer or multilayer atomic thickness, most of the neutrons directly penetrate through 2DMs into the substrates; only a few neutrons induce elastic scatterings[19)] (collisions) in the 2DMs. These elastic scatterings induce displacements of atoms from the lattice sites and create recoil atoms.[18)] The recoil atoms and the penetrating neutrons mainly cause cascading scatterings inside the substrates. Therefore for 2DMs we can omit the cascading scatterings and only consider the displacements and ionization generated by the primary collision of neutrons.[5)] What is more, due to their small size and electric neutrality, neutrons are very unlikely to create defects larger than a single vacancy compared with ion irradiation. Instead, they are expected to generate point defects with quasi-homogeneous distribution.[18)] These defects including their evolution process have crucial impacts on the electrical and optical features of MoS_2 materials and devices. To the best of our knowledge, this work is the first to investigate the defects and disorders of monolayer MoS_2 generated by fast-neutron irradiation. We conducted studies with photoluminescence (PL), Raman spectra and X-ray photoelectron spectroscopy (XPS). The results provide important information and facilitate a deeper understanding of MoS_2 performance under extreme conditions.

For the preparation of monolayer MoS_2, there are two typical methods: physical stripping and CVD growth. Here we use our previous CVD method[20)] which produces large-area, high-quality monolayers and heterostructures.[21,22)] MoS_2 was synthesized at a temperature of 830 °C on a sapphire substrate. A molybdenum oxide precursor was loaded into the center of a furnace and placed under the substrate. S powder in a separate vessel was located upstream with a heating belt system. CVD was performed under atmospheric pressure with an Ar flow rate of 500 sccm. After a 20 min reaction, the furnace was naturally cooled down to room temperature. Figure 1(a) shows an optical image of the CVD-grown MoS_2. The thicknesses of the samples were measured in AC air topography mode under an Asylum Research MFP-3D atomic force microscope (AFM), as shown in Fig. 1(b). The measured heights of the samples were about 1 nm, indicating a single-layer feature.[23,24)] Besides, Raman and PL spectra were obtained with a WITec alpha300 R confocal Raman microscope with a laser wavelength of 532 nm, as shown in Fig. 1(c). The two Raman peaks around 385.5 and 405.8 cm^{-1} correspond to the in-plane E^1_{2g} and out-of-plane A_{1g} modes of the monolayer MoS_2. The position difference (Δ) is about 20.8 cm^{-1}, further confirming the monolayer thickness of the sample.[23)] In addition, a single narrow PL peak around 1.874 eV (667 nm) corresponds to the A direct excitonic transition of monolayer MoS_2.[1,25)] The spatial dependences of the Raman and PL peak intensity mappings are shown in

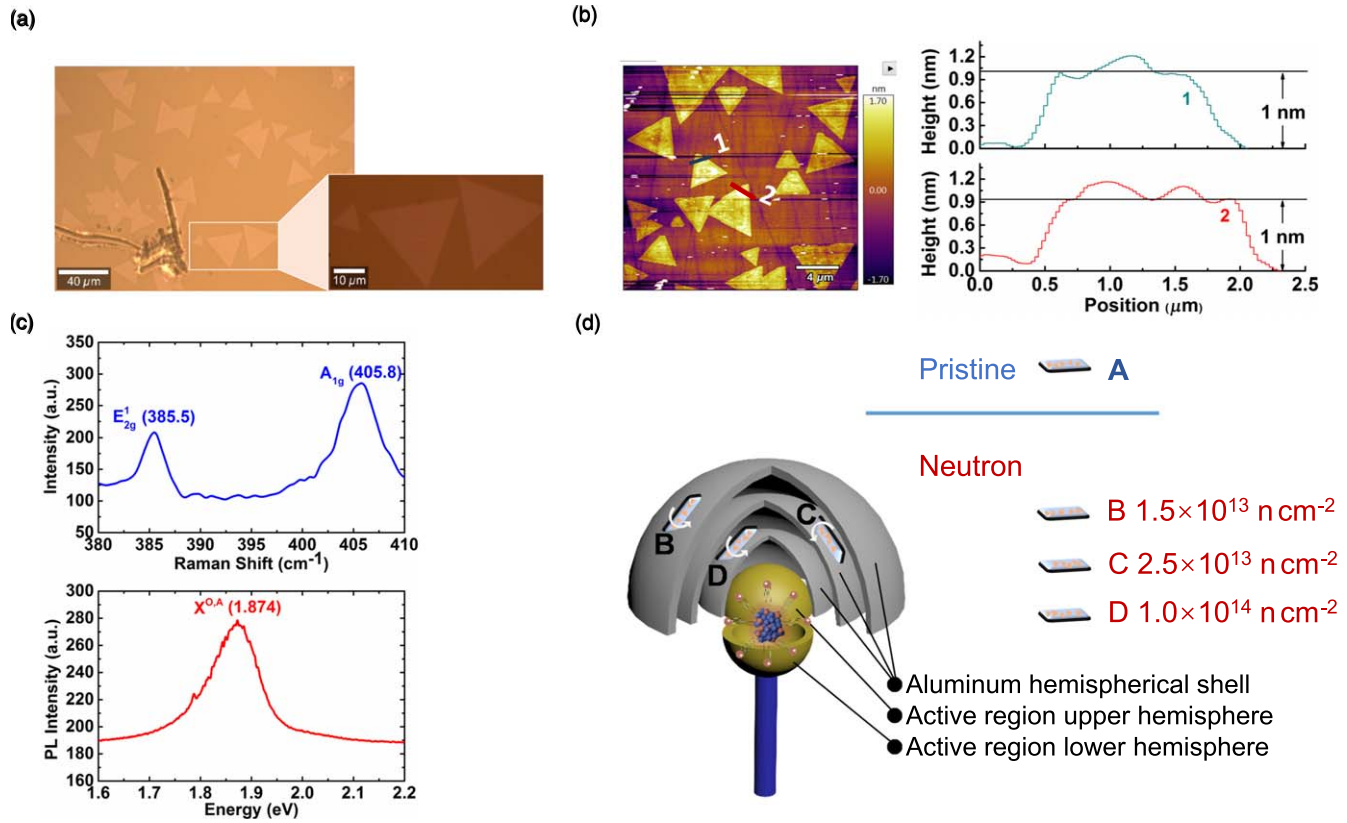

Fig. 1. (Color online) (a) Optical images of the CVD-grown MoS_2. (b) AFM image of the monolayer MoS_2 film on a sapphire substrate; the heights are about 1 nm from the AFM cross-sectional profile along the line (1 and 2). (c) Raman and PL spectra of monolayer MoS_2. (d) Positions of the samples and their corresponding neutron fluxes for the actual experiment. The sides of the MoS_2 were placed facing the neutron irradiation.

Fig. S1, available online at stacks.iop.org/APEX/12/056001/mmedia, further demonstrating the uniform thickness and similar optical quality of our as-grown monolayer MoS_2. In experiments, three Al shells were used to obtain different neutron fluxes of 1.5×10^{13}, 2.5×10^{13}, and 1.0×10^{14} n cm^{-2}, respectively. The average energy of the neutrons was 1.2 MeV, and the FWHM was 200 μs. Before irradiation, the sample consisted of a sapphire substrate with the as-grown monolayer MoS_2 cut into four segments (labeled A, B, C, and D). The four segments were placed in positions with various neutron fluxes as shown in Fig. 1(d): A was the pristine group, and B, C, and D were of the neutron irradiation group. Before neutron irradiation, positions of the A, B, C, and D segments with similar PL and Raman features were selected and marked as shown in Fig. S2.

Figure 2(b) shows the normalized PL spectra of the four tested samples over the amplitude of the sapphire substrate peak at 1.79 eV[26] with different neutron fluxes. In order to reduce the randomness of the single-point PL spectra, PL mappings with A-exciton ($X^{O,A}$) peak intensity were obtained as shown in Fig. 2(a). Both figures indicate that $X^{O,A}$ peak intensity drastically decreased with stronger neutron flux. In addition, by comparing the PL intensity mappings of the pristine monolayer MoS_2 sample with those of the irradiated samples, a significant PL peak intensity reduction with increasing neutron flux was observed. Compared to the $X^{O,A}$ peak, the intensity of the B-exciton ($X^{O,B}$) changed only slightly with the increase of neutron flux. Eventually, this led to obvious double peaks as shown in Fig. 2(b), and the contribution of the $X^{O,B}$ peak gradually went up with the

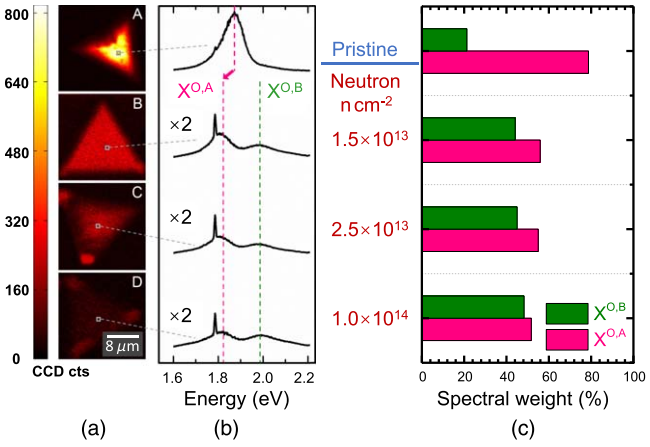

Fig. 2. (Color online) (a) PL intensity mappings of the four segments with the A-exciton ($X^{O,A}$) peak (sum from 1.77 eV to 1.94 eV for the PL spectra); the intensity drastically decreased with stronger neutron flux. (b) PL spectra of monolayer MoS_2 after neutron irradiation. The rectangles are the detection positions. (c) Spectral weight of the $X^{O,A}$ and B-exciton ($X^{O,B}$) peak contributions with neutron flux.

increase of neutron flux as shown in Fig. 2(c). With even higher neutron flux, the monolayer MoS_2 sample structure was destroyed, the peaks of $X^{O,A}$ and $X^{O,B}$ vanished and the contributions tended towards 50%.

Besides the PL intensity, there were red-shifts of the $X^{O,A}$ peaks as shown in Fig. 2(b). The red-shifts could have been induced by many factors, such as the layer number,[1] S and Mo vacancies,[27,28] adjoining parallel S vacancy lines (SVLs)[29] and the replacement of S atoms by O atoms.[30] The PL and Raman characteristics of the MoS_2 segments

before neutron irradiation rule out the possibility of a multilayer structure. S and Mo vacancies can introduce defect states and lead to a transition from a direct to an indirect bandgap. Meanwhile, the indirect bandgaps were lower than the original direct bandgap.[28] These can well explain the observed red-shift of $X^{O,A}$ and PL quenching. Although the band structures of SVLs with different widths also manifest lower bandgaps,[29] they are direct bandgaps which will not cause PL quenching. So the possibility of SVLs is eliminated. The replacement of S atoms by O atoms can change the band states from a direct to an indirect bandgap structure,[30] which could have also occurred.

To further prove this point, we tested the Raman characteristics of the four segments of the sample after neutron irradiation and the calculated Raman spectra of defective MoS_2 according to Ref. 9 are shown in Fig. 3. The peak widths of the E^1_{2g} mode and A_{1g} mode show significant broadening of the B, C, and D segments. For neutron flux of 1.5×10^{13} n cm^{-2}, the FWHM of the A_{1g} mode broadens from 4 to 18 cm^{-1}. This phenomenon was also observed in single-layer MoS_2 via O plasma treatment,[30] which may have resulted from O defect sites[31] and lattice disorder in MoS_2. Besides, red-shifts of the peak positions of E^1_{2g} and A_{1g} are observed, and the peak positions of E^1_{2g} and A_{1g} are close to the peak positions of the calculated Raman spectra of defective MoS_2 with Mo vacancies, indicating the formation of Mo vacancies. The peak around 440–460 cm^{-1} is a fingerprint of the formation of S vacancies.[9] Since neutron volume is much lower than that of ion (such as in Ar ion irradiation), the probability of cascading scattering events in monolayer MoS_2 is low; then the creation of MoS_6 vacancies could be ignored.[9,32] Therefore, we can conclude that for neutron irradiation, the defects of monolayer MoS_2 are dominated by atomic defects (S and Mo vacancies) and O defect sites.

To investigate the chemical states of Mo and S vacancies on the surface of the sample, we conducted XPS by a Thermo Scientific™ ESCALAB™ Xi$^+$ with an X-ray spot size of 400 μm. The XPS spectra were calibrated by the C 1s peak located at 284.5 eV.[33] Figure 4(a) illustrates the peaks of the sapphire substrate which included 553.2 eV (O loss), 531.1 eV (O 1s), 117.9 eV (Al 2s), 103.7 eV (Al loss), and 73.1 eV (Al 2p). The scan spectra were fitted by Thermo Avantage software using the Powell optimization algorithms and Gaussian–Lorentzian functions. As shown in Fig. 4(b), the Mo $3d_{3/2}$ and Mo $3d_{5/2}$ peaks moved to lower binding energy with stronger neutron flux, and a MoO_3 peak at 235.5 eV was observed, indicating the formation of a Mo^{6+} oxidation state. The MoO_3 peak appearing at 1.0×10^{14} n cm^{-2} illustrates the S atoms were moved out of the lattice due to the neutron irradiation, and the oxidation took the place of the S vacancies.[30,34] Moreover, we

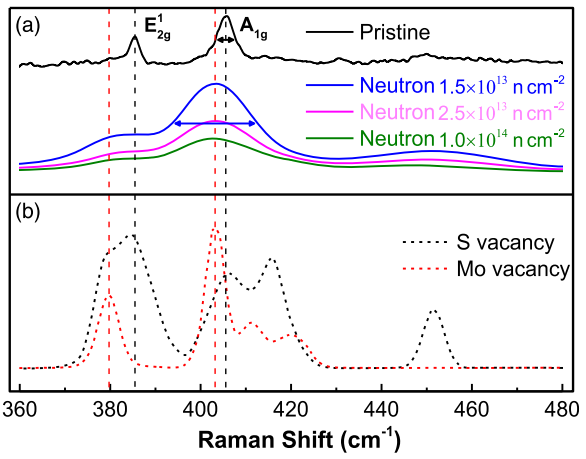

Fig. 3. (Color online) (a) Raman characterizations of the four segments of the sample after neutron irradiation. (b) Calculated Raman spectra of defective MoS_2.[9]

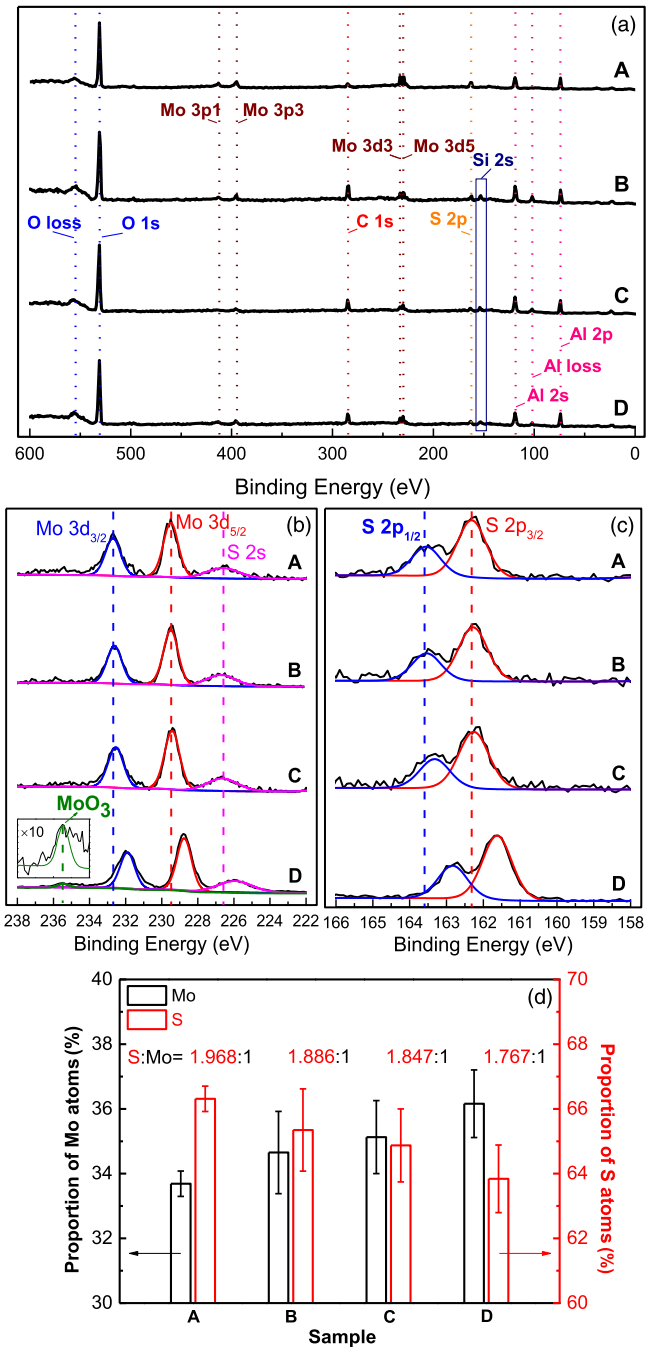

Fig. 4. (Color online) (a) XPS survey spectra of monolayer MoS_2 before and after neutron irradiation, including O, Mo, C, S, and Al peaks. (b) XPS scan spectra of Mo 3d and S 2s peaks. A MoO_3 peak is shown in the inset image. (c) XPS scan spectra of S 2p peaks. (d) The proportions of S and Mo atoms, and the relative atomic content ratio of S to Mo (S:Mo) before and after neutron irradiation. Sample A is the pristine group; samples B, C and D are the neutron irradiation groups at 1.5×10^{13}, 2.5×10^{13}, and 1.0×10^{14} n cm^{-2}.

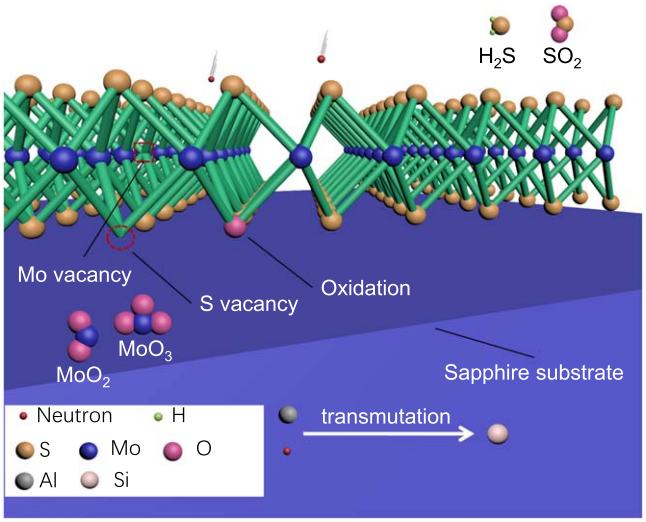

Fig. 5. (Color online) Atomic structure of monolayer MoS_2 with Mo and S vacancies under fast-neutron irradiation; the oxidation took the place of the S vacancy. Proposed products of displaced S and Mo atoms, and transmutation-produced Si impurity from the fast-neutron reaction with Al.

observed the red-shift of the S $2p_{1/2}$ and S $2p_{3/2}$ XPS peaks; these evolutions of the Mo 3d peaks and S 2p peaks under neutron irradiation are similar to chloride ion bombardment,[35] further indicating a Mo^{4+} oxidation state.

It is worth noting that neutron irradiation leads to material activation[36] and radioactivity. Under considerations of safety, the samples were taken out a week after the radiation experiments to ensure their radioactivity had reduced to safe dose levels. In order to exclude the influence of natural oxidation, all four samples were characterized after the same waiting period and in the same characterization period. We also observed a new peak at 153 eV (Si 2s) after neutron irradiation as illustrated in Fig. 4(a), which was caused by a transmutation-produced Si impurity from the fast-neutron reaction with Al.[37] In addition, the relative atomic content ratio of S to Mo (S:Mo) decreased with higher neutron flux, which can be seen in Fig. 4(d). However, the displacement cross-section[38,39] ratio of S to Mo was 3:4; this means the collision probability between Mo atoms and neutrons was larger than that between S atoms and neutrons, and the ratio went up with an increasing flux of neutrons. We attribute the decrease of the ratio to the release of S atoms, such as simple gases (SO_2,[30,34] H_2S[40]) and volatile species.[41] The displaced Mo atoms remained on the surface of the samples by oxidation or other means, as shown in Fig. 5. Neutron irradiation produced a number of S and Mo vacancies in an extremely short period, and oxidation products of the displaced S and Mo atoms were generated accordingly. This process is different from oxygen substitution under ambient conditions,[42] and accelerates the degradation of 2DM performance.

In conclusion, we investigated the neutron irradiation effects on monolayer MoS_2. The features of the PL spectra, Raman spectra and XPS of monolayer MoS_2 irradiated with fast neutrons were carefully interpreted. In the PL spectra, the A-exciton ($X^{O,A}$) peak showed a red-shift and its intensity significantly decreased with an increasing flux of neutrons, which was caused by S and Mo vacancies, and by the oxidation replacement of the S vacancies. The Raman results exhibited red-shifts and broadenings of the E^1_{2g} mode and A_{1g} mode which also proved the formation of S and Mo vacancies. The shiftings of the Mo 3d peaks and S 2p peaks, and the appearance of a MoO_3 peak in the XPS spectra confirmed the oxidation took the place of the S vacancies. These results provide a basis for a fundamental understanding of the optical properties of MoS_2 under neutron irradiation, and supply supporting information for the development and evaluation of radiation-hardened MoS_2-based devices.

Acknowledgments This work was supported by the Science Challenge Project (TZ2016003-2), Fundamental Research Funds for the Central Universities of China (Grant Nos. 2018CDGFGD0008 and 10611CDJXZ238826), Grant for Science and Technology Innovation in Chongqing of China (Grant No. cstc2017shmsA00004), the National Natural Science Foundation of China (Grant No. 61705203), and Singapore A*STAR AME IRG (Grant No. A1783c0011).

ORCID iDs Ge Tang https://orcid.org/0000-0002-8778-2871

1) K. F. Mak, C. Lee, J. Hone, J. Shan, and T. F. Heinz, Phys. Rev. Lett. **105**, 136805 (2010).
2) F. Nan, K. Nagashio, and A. Toriumi, Appl. Phys. Express **8**, 65203 (2015).
3) Y. Iwasa, Y. Saito, Y. Kasahara, J. Ye, and T. Nojima, Science **350**, 409 (2015).
4) S. Xiong and G. Cao, Nanotechnology **26**, 185705 (2015).
5) R. C. Walker, T. Shi, E. C. Silva, I. Jovanovic, and J. A. Robinson, Phys. Status Solidi **213**, 3268 (2016).
6) R. Branimir and K. Andras, Nat. Mater. **12**, 815 (2013).
7) S. Mouri, Y. Miyauchi, and K. Matsuda, Nano Lett. **13**, 5944 (2013).
8) H. Guo, Y. Sun, P. Zhai, H. Yao, J. Zeng, S. Zhang, J. Duan, M. Hou, M. Khan, and J. Liu, Appl. Phys. A **122**, 375 (2016).
9) S. Bae, N. Sugiyama, T. Matsuo, H. Raebiger, K. I. Shudo, and K. Ohno, Phys. Rev. Appl. **7**, 024001 (2017).
10) J. Zhang, H. Ouyang, X. Zheng, J. You, R. Chen, T. Zhou, Y. Sui, Y. Liu, X. Cheng, and T. Jiang, Opt. Lett. **43**, 243 (2018).
11) R. Rani, D. Sharma, N. Jena, A. Kundu, A. D. Sarkar, and K. S. Hazra, Appl. Phys. Lett. **110**, 196803 (2017).
12) H. M. Oh, G. H. Han, H. Kim, J. J. Bae, M. S. Jeong, and Y. H. Lee, ACS Nano **10**, 5230 (2016).
13) B. Ozden, K. Min, J. Park, S. Uprety, V. Mirkhani, K. Yapabandara, K. Kim, M. Kuroda, M. Bozxack, and W. Choi, Micro Nano Lett. **12**, 271 (2017).
14) A. R. Sweedler, D. E. Cox, and S. Moehlecke, J. Nucl. Mater. **72**, 50 (1978).
15) I. S. Shlimak, Phys. Solid State+ **41**, 716 (1999).
16) D. S. Hamm, M. Rust, E. H. Herrera, L. Matei, V. Buliga, M. Groza, A. Burger, A. Stowe, J. Preston, and E. D. Lukosi, Appl. Phys. Lett. **112**, 242104 (2018).
17) N. Wakabayashi, H. G. Smith, and R. M. Nicklow, Phys. Rev. B **12**, 659 (1975).
18) D. I. Tetelbaum, D. V. Guseinov, V. K. Vasiliev, A. N. Mikhaylov, A. I. Belov, D. S. Korolev, S. V. Obolensky, and A. N. Kachemtsev, Nucl. Instrum. Meth. B **326**, 41 (2014).
19) K. Senoo, Y. Nagai, T. Shima, T. Ohsaki, and M. Igashira, Nucl. Instrum. Meth. A **339**, 556 (1994).
20) M. E. Pam et al., J. Phys. Chem. Lett. **10**, 1292 (2019).
21) Y. H. Lee, X. Q. Zhang, W. Zhang, M. T. Chang, C. T. Lin, K. D. Chang, Y. C. Yu, J. T. Wang, C. S. Chang, and L. J. Li, Adv. Mater. **24**, 2320 (2012).
22) L. Keng-Ku, Z. Wenjing, L. Yi-Hsien, L. Yu-Chuan, C. Mu-Tung, S. Ching-Yuan, C. Chia-Seng, L. Hai, S. Yumeng, and Z. Hua, Nano Lett. **12**, 1538 (2012).
23) H. Li, Q. Zhang, C. C. R. Yap, B. K. Tay, T. H. T. Edwin, A. Olivier, and D. Baillargeat, Adv. Funct. Mater. **22**, 1385 (2012).
24) R. F. Frindt, J. Appl. Phys. **37**, 1928 (1966).
25) A. Splendiani, L. Sun, Y. Zhang, T. Li, J. Kim, C. Y. Chim, G. Galli, and F. Wang, Nano Lett. **10**, 1271 (2010).
26) H. Chung-Che, A. S. Feras, W. Yudong, O. Jun-Yu, J. C. Walker, W. Shuncai, G. Behrad, R. E. Simpson, and D. W. Hewak, Nanoscale **6**, 12792 (2014).
27) H. Qiu, T. Xu, Z. Wang, W. Ren, H. Nan, Z. Ni, Q. Chen, S. Yuan, F. Miao, and F. Song, Nat. Commun. **4**, 2642 (2013).

28) C. González, B. Biel, and Y. J. Dappe, Nanotechnology **27**, 105702 (2016).
29) S. Wang, G. D. Lee, S. Lee, E. Yoon, and J. H. Warner, ACS Nano **10**, 5419 (2016).
30) N. Kang, H. P. Paudel, M. N. Leuenberger, L. Tetard, and S. I. Khondaker, J. Phys. Chem. C **118**, 21258 (2014).
31) J. Yang, S. Kim, W. Choi, S. H. Park, Y. Jung, M. H. Cho, and H. Kim, ACS Appl. Mater. Interfaces **5**, 4739 (2013).
32) S. Yuan, R. Roldán, M. I. Katsnelson, and F. Guinea, Phys. Rev. B **90**, 041402 (2014).
33) W. Haotian, L. Zhiyi, X. Shicheng, K. Desheng, J. J. Cha, Z. Guangyuan, H. Po-Chun, Y. Kai, B. David, and F. B. Prinz, Proc. Natl. Acad. Sci. **110**, 19701 (2013).
34) M. R. Islam, K. Narae, B. Udai, H. P. Paudel, E. Mikhail, T. Laurene, M. N. Leuenberger, and S. I. Khondaker, Nanoscale **6**, 10033 (2014).
35) R. Murray, K. Haynes, X. Zhao, S. Perry, C. Hatem, and K. Jones, ECS J. Solid State Sci. Technol. **5**, Q3050 (2016).
36) V. I. Pavlenko, R. N. Yastrebinskii, and D. V. Voronov, J. Eng. Phys. Thermophys. **81**, 686 (2008).
37) R. T. King, E. L. L. Jr, J. O. Stiegler, and K. Farrell, J. Nucl. Mater. **35**, 231 (1970).
38) W. Yin, T. J. Liang, Q. Z. Yu, and X. J. Jia, J. Nucl. Mater. **398**, 100 (2010).
39) L. Wang, X. Pan, Y. Zhu, G. Zhu, X. Jiang, Y. Feng, X. Zhang, and Z. Zhang, Nucl. Technol. **36**, 110204 (2013).
40) J. F. Paul and E. Payen, J. Phys. Chem. B **107**, 4057 (2003).
41) B. X. Liu, X. Q. Pei, Q. H. Wang, X. J. Sun, and T. M. Wang, Appl. Surf. Sci. **258**, 1097 (2011).
42) P. János, O. Tamás, V. Péter, I. P. Zakhar, Z. M. Gábor, D. Gergely, H. Chanyong, B. S. Pavel, and T. Levente, Nat. Chem. **10**, 1246 (2018).